DOI: 10.1002/ejic.200801216

Minerals as Model Compounds for Cu/ZnO Catalyst Precursors: Structural and Thermal Properties and IR Spectra of Mineral and Synthetic (Zincian) Malachite, Rosasite and Aurichalcite and a Catalyst Precursor Mixture

Malte Behrens,*[a] Frank Girgsdies,[a] Annette Trunschke,[a] and Robert Schlögl[a]

Keywords: Copper / Zinc / Heterogeneous catalysis / X-ray diffraction / Thermochemistry

The Cu/ZnO system is a model for Cu/ZnO/Al_2O_3 catalysts, which are employed industrially for the synthesis of methanol. These catalysts are usually prepared from mixed basic carbonate precursors. A complex phase mixture, with constituents structurally related to the minerals rosasite and aurichalcite, is present at the industrially applied composition (Cu/Zn ≈ 70:30). Using minerals and phase-pure synthetic samples as references, a comprehensive characterisation of such a phase mixture, including the determination of the individual compositions of the different phases, has been attempted by complementary analytical laboratory techniques (XRD, TGA, IR). The results are critically discussed in light of the complexity of the system. A thermally very stable carbonate species − well-known for mixed synthetic systems − is also detected for the mineral reference samples. Significant amounts of amorphous phases are found to be present in the synthetic zincian malachite sample but not in synthetic aurichalcite or the catalyst precursor. A simplified explanation for the shift of the characteristic $20\bar{1}$ reflection of the malachite structure as a function of Zn incorporation based on the varying average Jahn–Teller distortion of the MO_6 octahedra is proposed.

Introduction

Copper-based catalysts are widely employed in methanol synthesis and the water gas shift reaction. They are also active in other reactions, such as steam reforming of methanol. Industrially applied Cu/ZnO/Al_2O_3 catalysts exhibit an Cu/Zn atomic ratio of approximately 70:30 and contain 5–10 at.-% Al_2O_3 as an additional phase. An effective and industrially applied preparative route for these catalysts is via a multi-step synthesis involving co-precipitation of mixed Cu/Zn hydroxycarbonate precursors, calcination to give a mixture of oxides and reduction of the CuO component. A vast number of studies on this system, performed by many different research groups, have shown that the synthetic parameters during the very early stages of the preparation process crucially affect the physicochemical properties of the precursor material[1–12] and, in turn, the catalytic activity of the final catalyst. This phenomenon is termed the "chemical memory" of the system. A comprehensive knowledge of the properties of the co-precipitated precursor material is therefore highly desirable for further optimisation of the catalyst.

A mixed solution of Cu/Zn nitrate and sodium carbonate is often used as a precipitating agent for the successful co-precipitation of Cu/Zn hydroxycarbonate precursors. The precipitation parameters, especially composition, temperature, concentration, mode of precipitation (e.g. constant, decreasing or increasing pH) or time of aging in the mother liquor, are well known to have a significant impact on the product's properties and their optimal setting is usually determined on the basis of trial-and-error processes. More rational approaches are hindered by difficulties in completely characterising the precursor material. These difficulties arise from the fact that: i) the material is seldom phase-pure; ii) it is usually only poorly crystalline, thereby limiting the information available from diffraction techniques; iii) the similar X-ray scattering power of Cu and Zn does not allow their discrimination by means of conventional X-ray diffraction (XRD); iv) the phases present usually exhibit a broad range of possible Cu/Zn ratios, thus making an unambiguous determination of their individual compositions very difficult; v) the ratio of the CO_3^{2-} and OH^- anions, as well as the amount of structure water, may vary; and vi) the material is usually sensitive to decomposition under irradiation of an electron beam, thereby complicating the characterisation by high resolution TEM. It is therefore clear that these problems can only be tackled by applying several complementary characterisation techniques, and comprehensive results have already been reported, for example, for a 2:1 Cu/Zn system.[2] The situation is usually simplified by regarding the precursor mixture as being composed of various fractions of well-defined mineral reference materials and considering its properties as a superimpo-

[a] Fritz Haber Institute of the Max Planck Society, Department of Inorganic Chemistry,
Faradayweg 4–6, 14195 Berlin, Germany
Fax: +49-30-8413-4405
E-mail: Behrens@fhi-berlin.mpg.de

sition of their characteristics. The goal of this study is: i) to provide information on the properties of single-phase precipitates and mineral reference compounds acquirable by standard laboratory techniques, (ii) to identify the advantages and shortcomings of the "mineral approach" by comparison with the real precursor mixture, and (iii) to try to use this information to fully characterise the latter and critically discuss the results. In this contribution, we restrict ourselves to binary Cu/ZnO samples which serve as a suitable model for the technical ternary $Cu/ZnO/Al_2O_3$ system.

The crystalline components of the precursor material are usually identified by XRD as being structurally related to the mineral phases (zincian) malachite, rosasite and aurichalcite. Herein, we report the structural and thermal characteristics and IR spectra of these mineral reference compounds and compare the results with precipitated single-phase samples and a phase mixture with a 70:30 Cu/Zn ratio representative of the typical technical system. The spectroscopic properties of these samples in the UV/Vis/NIR range will be presented in a forthcoming paper.

Results and Discussion

Minerals and Synthetic Single-Phase Samples

Crystal Structures and Compositions

The crystal structures of the minerals malachite, rosasite and aurichalcite have been reported in the literature.[13–17] The most important structural features are briefly discussed here. Malachite $[Cu_2(CO_3)(OH)_2]$ crystallises in the monoclinic space group $P2_1/a$ (a = 9.502, b = 11.974, c = 3.240 Å; β = 98.75°; V = 364.35 Å^3).[13,14] The two crystallographically independent metal positions Cu1 and Cu2 are coordinated by six oxygen atoms in a Jahn–Teller distorted octahedral [4+2] environment. The Cu1 octahedra exhibit a more pronounced distortion, with axial Cu–O distances of 2.51 and 2.64 Å, whereas the axial Cu2–O spacing amounts to 2.37 Å. All equatorial Cu–O distances are within the range 1.90–2.11 Å. The Cu1 and Cu2 octahedra are connected via common edges to form double chains running parallel to the c-axis. Adjacent double chains share common corners to form wavy layers in the (101) planes. These layers are connected in the b-direction via carbonate groups (Figure 1, a).

Rosasite $[(Cu,Zn)_2(CO_3)(OH)_2]$ crystallizes in the monoclinic space group $P2_1/a$ (a = 12.873, b = 9.354, c = 3.156 Å; β = 110.36°; V = 356.3 Å^3 for a sample with Cu/Zn = 1.44:1)[15] and its structure is closely related to that of malachite, as suggested by the similar XRD patterns of the two samples. Due to the usually small and fibrous crystallites, no refinement of a single crystal structure has been reported so far, but recent powder diffraction work[16] suggests that the connectivity of the octahedra is similar to that in malachite, although a clear Jahn–Teller distortion is absent for the $M2O_6$ units and is weaker for the $M1O_6$ units (axial M–O: 2.44 and 2.52 Å; equatorial M–O: 1.90–2.08 Å) than for $Cu1O_6$ in malachite. The Cu content of naturally occurring rosasite ([Cu]/[Cu+Zn]) is normally 33–50%.[18] The Zn content of our mineral rosasite sample was determined by SEM-EDX and amounts to 38% of total metal. Synthetic $[(Cu,Zn)_2(CO_3)(OH)_2]$ samples can be prepared with Zn contents as low as 0%.[4–6,8,12] Such low-Zn materials are often denoted zincian malachite. According to Perchiazzi,[16] the crystallographic difference between (zincian) malachite and rosasite is related to the different orientation of the space group symmetry operators, which leads to two distinct structures. However, an unambiguous discrimination on the basis of the powder XRD patterns of poorly crystalline precipitated samples is difficult due to the high similarity of the crystal structures. In the field of catalysis research, the differences in the long-range order of malachite and rosasite are therefore often neglected and the terms zincian malachite and rosasite are used synonymously. Malachite and rosasite are regarded as boundary cases in a pseudo-isomorphous substitution series of Zn^{2+} into $[(Cu_{1-x}Zn_x)_2(CO_3)(OH)_2]$, although the exact value of

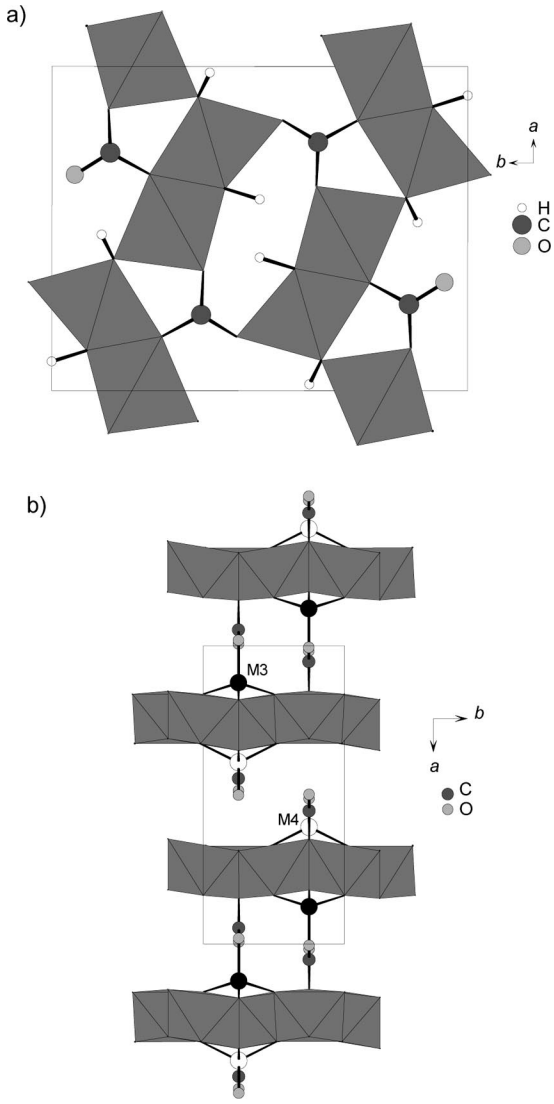

Figure 1. a) Crystal structure of malachite viewed along [001]; b) crystal structure of aurichalcite viewed along [001].

x often remains undetermined. Using the decreasing pH co-precipitation method, we have been able obtain crystallographic phase-pure samples with nominal Zn contents close to 10%; a higher Zn content in the solution leads to the formation of aurichalcite [$(Cu,Zn)_5(OH)_6(CO_3)_2$] as a by-phase.[12]

Aurichalcite is structurally related to the pure Zn mineral hydrozincite [$Zn_5(OH)_6(CO_3)_2$] and crystallizes in the monoclinic space group $P2_1/m$ (a = 13.82, b = 6.419, c = 5.29 Å; β = 101.04°; V = 460.59 Å^3).[17] This single-crystal structure was determined for a sample containing 40% Cu. The unit cell contains four crystallographically independent metal sites (M1–M4). M1 and M2 are octahedrally coordinated by six oxygen atoms. The $M2O_6$ unit is Jahn–Teller distorted and exhibits equatorial M–O distances of around 2 Å, whereas the axial ones measure 2.31 and 2.38 Å. The $M1O_6$ octahedron exhibits three different M–O spacings of between 1.94 and 2.24 Å but no significant elongation of any single axis. M3 is tetrahedrally coordinated by four oxygen atoms and M4 is located in a fivefold distorted trigonal-bipyramidal environment. The octahedra are connected by common edges to form layers parallel to the (011) planes. One out of every four octahedra is missing and M3- and M4-centred units are found at this position on either side of the layer. The $M3O_4$ tetrahedra connect two adjacent layers via carbonate to form double layers, which are connected to each other solely by hydrogen bonding (Figure 1, b). Natural aurichalcite contains 24–40% Cu.[19] The Cu content of our mineral sample was determined by SEM-EDX to be 32%. Synthetic aurichalcite was prepared with a nominal Cu content of 33%.

Vibrational Spectroscopy

IR spectroscopy is sensitive to molecular structure and is capable of probing both the amorphous and crystalline parts of the samples, which means that it is complementary to XRD. The FTIR spectra of the samples were recorded at room temperature and Figure 2 shows a comparison of the hydroxide, carbonate and fundamental mode fingerprint regions of the IR spectra for all five samples.

Stretching bands for O–H are observed in the range 4500–2500 cm^{-1} (Figure 2, a). The spectrum of malachite shows a typical splitting into two modes at 3318 and 3407 cm^{-1}, which is attributed to the two crystallographically different OH groups.[20] The O–H bands for rosasite are less intense and the splitting is strongly enhanced to 251 cm^{-1}. A correlation between the splitting of these O–H stretching bands and the degree of Zn incorporation in the malachite structure has been reported in the literature.[21] The spectrum of mineral aurichalcite exhibits a single broad band centred at around 3325 cm^{-1}, whereas an additional sharper absorption band is observed at 3387 cm^{-1} in the spectrum of the synthetic aurichalcite sample, thus indicating the presence of an OH-containing species not present in the mineral.

The ν_3 (asymmetric C–O stretching) mode of the carbonate anions appear in the region 1700–1100 cm^{-1} (Figure 2, b). Four bands are observed for malachite[22] at 1520 (shoulder), 1494, 1423 and 1388 cm^{-1} due to correlation field splitting. For the synthetic zincian malachite sample, the first two bands are not resolved and a single broader band appears at 1513 cm^{-1}. The other two bands are

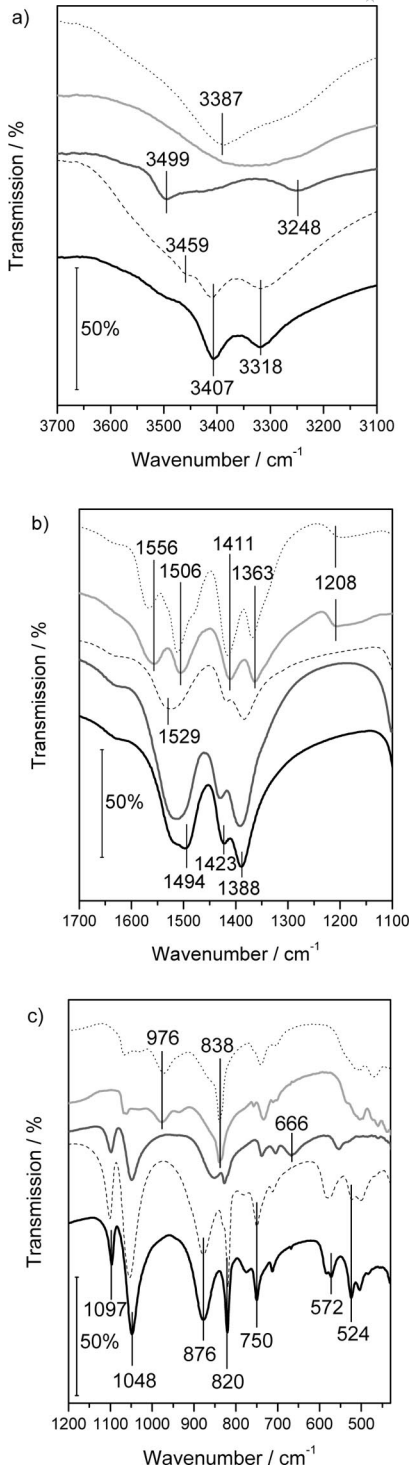

Figure 2. IR spectra of minerals malachite (black), rosasite (dark grey) and aurichalcite (light grey) and the synthetic samples zincian malachite (dashed) and aurichalcite (dotted) in the ranges: a) 3700–3100 cm^{-1}, b) 1700–1100 cm^{-1}, and c) 1100–400 cm^{-1}. The spectra are offset by an arbitrary amount for clarity.

slightly shifted to higher wavenumber. The spectrum of mineral rosasite is very similar, but the broad band at high wavenumber is shifted by 15 cm^{-1} to higher wavenumber and the doublet at lower wavenumber by 10 cm^{-1} to lower wavenumber. On the basis of our samples, no clear correlation between the spectral features in this region and the Zn content of the samples crystallizing in the malachite/rosasite structure can be established.

In agreement with the literature data,[23] four bands of almost equal intensity are observed for mineral aurichalcite at 1556, 1506, 1411 and 1363 cm^{-1}. These bands are found at slightly higher wavenumbers in the spectrum of the synthetic aurichalcite sample, although the intensity pattern differs between the mineral and synthetic samples. Thus, the two inner bands in the spectrum of the latter are significantly more intense than the two outer ones. Additionally, shoulders to the higher and lower wavenumber sides of the band centred at 1512 cm^{-1} appear for the synthetic samples. Such a fine structure is not observed for the mineral. The carbonate ν_3 bands originating from the malachite/rosasite and aurichalcite structure overlap significantly, therefore characterisation of a phase mixture on the basis of this spectral region will be complicated. The band at 1208 cm^{-1}, however, is a clear fingerprint feature of the aurichalcite structure as it is present in mineral and synthetic aurichalcite but not for the malachite/rosasite samples. It has been pointed out previously in the literature that this band, which has been assigned to an M–OH deformation vibration,[24] can be used to identify aurichalcite in a phase mixture.[4]

OH deformation vibrations and further carbonate bands can be found in the range 1200–600 cm^{-1} (Figure 2c). The vibrations of the M–O skeleton are observed below 600 cm^{-1}.[25] The spectrum of the mineral malachite exhibits three strong OH libration bands at 1097, 1048 and 876 cm^{-1}. According to Schmidt at al.,[20] the symmetric C–O stretching vibration of carbonate (ν_1), which is IR active due to the lowered symmetry for coordinated carbonate, is expected at 1085 cm^{-1} but masked by the strong OH deformation bands. The carbonate modes ν_2 and ν_4 (out-of-plane and asymmetric O–C–O bending, respectively) are observed as a sharp band at 817 cm^{-1} and a triplet at around 750 cm^{-1}, respectively. The only slight difference between mineral malachite and synthetic zincian malachite is a weak shift of the first two OH deformation bands to higher wavenumber. For the mineral rosasite, it is the third OH deformation band which is shifted by 24 cm^{-1} to lower wavenumber. The carbonate bands are similar for the mineral malachite sample and the synthetic zincian malachite. For rosasite, ν_2 is shifted by 10 cm^{-1} and ν_4 by 12 cm^{-1} in opposite directions. A rosasite band is observed at 666 cm^{-1}, a position where no other sample shows any special feature. This relatively broad band can thus serve as a fingerprint for rosasite. The spectra of mineral and synthetic aurichalcite are similar in this region. In contrast to malachite, an OH deformation band is observed at 976 cm^{-1} for the mineral sample (970 cm^{-1} for the synthetic sample) and can be regarded as another suitable fingerprint band for the presence of aurichalcite in a phase mixture.[4] The carbonate bands ν_2 and ν_4 are located at 838 and 734 cm^{-1}, respectively, for the mineral sample, with the latter being shifted by 5 cm^{-1} to higher wavenumber for synthetic aurichalcite. The skeletal M–O vibrations at wavenumbers below 600 cm^{-1} are in good agreement for both minerals and synthetic samples, but clearly different for malachite and aurichalcite. The rosasite spectrum is unique in this range, thus indicating the pronounced sensitivity of M–O bands to the Cu/Zn ratio.

The IR spectra of synthetic and mineral samples show a reasonable degree of agreement, thereby confirming a similar local structure in precipitated and mineral materials. The differences between the three Cu-rich malachite-like samples, such as the band shifts, can be explained on the basis of their different Cu/Zn ratios. The differences between the spectrum of synthetic aurichalcite and that of the mineral sample are more pronounced, however, despite their similar nominal composition. Additional bands or shoulders are observed in the hydroxyl and carbonate fingerprint regions and strong deviations of the intensity pattern are detected. Although many bands of the different hydroxycarbonate structures overlap, IR spectroscopy provides a fingerprint method for discriminating malachite/rosasite and aurichalcite by means of the bands near 1200 and 970 cm^{-1}, which are unique to aurichalcite. Furthermore, mineral rosasite can be identified on the basis of the band at 666 cm^{-1}.

Thermal Properties

The thermal decomposition of the hydroxycarbonates was investigated by thermogravimetry (TG) and mass spectrometric (MS) evolved gas analysis. The TG-MS curves of mineral malachite are shown in part a of Figure 3. Malachite decomposes completely in a single step with the maximal rate of weight loss at around 350 °C. As expected, a simultaneous emission of water and carbon dioxide was detected, thus indicating decomposition of hydroxyl and carbonate species. The weight loss of 27.3% is slightly lower than the calculated value of 28.1% for complete transformation into CuO.

The decomposition curves of mineral rosasite are shown in Figure 3 (b). Here, the overall mass loss of 27.7% is in good agreement with the calculated value for complete dehydroxylation and decarbonation (27.9%). Interestingly, the decomposition proceeds in two consecutive steps, with the sample losing around 22% of its weight due to a simultaneous emission of water and carbon dioxide at around 400 °C. Whereas all hydroxy groups are decomposed after this step, some carbonate species not present in pure malachite resist thermal treatment at 400 °C and are emitted in a second decomposition step at a temperature of approximately 480 °C.

The decomposition of the mineral aurichalcite sample is qualitatively very similar to that of rosasite (Figure 3, c). Thus, whereas the overall mass loss of 26.0% is close to the

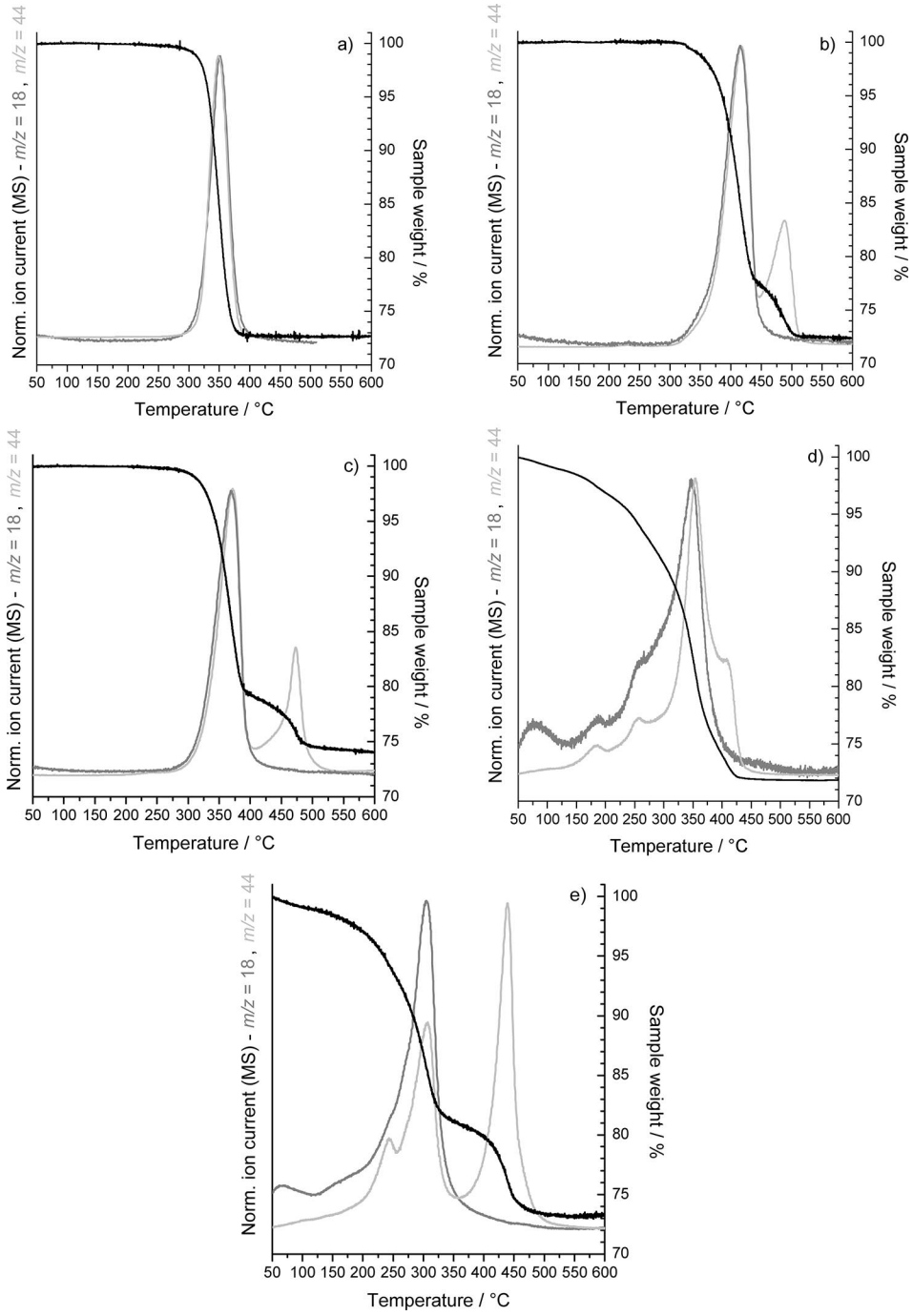

Figure 3. TG curves (black) and MS traces for H_2O (dark grey) and CO_2 (light grey) for: a) mineral malachite, b) mineral rosasite, c) mineral aurichalcite, d) synthetic zincian malachite, and e) synthetic aurichalcite.

theoretical value of 26.3%, a first simultaneous dehydroxylation and decarbonation step at around 370 °C is followed by a further decarbonation at 480 °C.

This so-called "high-temperature carbonate" is commonly observed in synthetic Cu/ZnO catalyst precursors prepared by co-precipitation.[8,12] Its abundance has been found to be a function of the Cu/Zn ratio and its positive effects on the catalytic properties of the resulting catalysts have been discussed.[26] To the best of our knowledge, these resistant carbonate species have not been reported for (Cu,Zn) minerals before. Their presence in our mineral samples suggests that these species are not necessarily formed during the precipitation process but might rather be an intrinsic property of mixed (Cu,Zn) hydroxycarbonates, particularly if they are well crystalline. The fraction of carbonate being decomposed at high temperature can be estimated to be 30% for rosasite and 35% for aurichalcite from the ratio of the areas under the two MS peaks at *m*/*z* 44. It should be noted, however, that the presence of different carbonate species is not evident from the rosasite crystal

structure, which, as is the case for malachite, exhibits only one crystallographically unique type of carbonate. Furthermore, it seems unlikely that the subtle crystallographic differences between rosasite and malachite are responsible for the severe discrepancies in their thermal properties. In aurichalcite, however, there are indeed two types of crystallographically distinct carbonate species, although their ratio is 50:50 and not near to 65:35. Hence, the crystal structures of the precursors do not provide a simple explanation for the presence of high-temperature carbonate. As it is only observed in mixed Cu/Zn systems, we rather suggest that high-temperature carbonate is trapped at the ZnO–CuO interfaces. In this model, the abundance and stability of high-temperature carbonate would be determined by the amount of interfaces and grain boundaries formed during the first decomposition step, which might explain the influence of composition and particle morphology on the decarbonation of mixed precursors. It should be noted that high-temperature carbonate was not reported for the pure Zn material hydrozincite [$Zn_5(OH)_6(CO_3)_2$].[4,12]

The thermal properties of the synthetic samples are shown in parts d and e of Figure 3. The zincian malachite decomposes in the temperature range 100–450 °C with a total mass loss of 28.3% (theoretical: 28.2%). The reaction consists of several poorly resolved simultaneous dehydroxylation and decarbonation steps at 180, 260 and 355 °C. The latter is the main decomposition event and can be compared to the single decomposition step observed for the mineral malachite sample, while the events at lower temperatures were not observed for the mineral sample. Dehydroxylation seems to be complete at 390 °C, whereas another decarbonation step at 405 °C indicates the presence of around 17% of a high-temperature carbonate species in this sample. This species decomposes at a considerably lower temperature than the Zn-richer samples. Synthetic aurichalcite is thermally less stable than the mineral material, with the main events happening at around 300 °C (simultaneous dehydroxylation and decarbonation) and 440 °C (decomposition of high-temperature carbonate). The fraction of high-temperature carbonate is higher and amounts to 52% of all carbonate species. Furthermore, an additional weak decarbonation step not found for the mineral is observed near 240 °C. The total mass loss of 26.9% is slightly higher than the calculated value of 26.3%.

In general, thermal treatment of single-phase (Cu,Zn) hydroxycarbonates results in a main decomposition step at 300–400 °C with simultaneous water and carbon dioxide emission. Another decarbonation step is observed at higher temperatures (>400 °C) for all samples containing Zn, whereas pure malachite also does not contain the high-temperature carbonate species. Since the thermal stability of solids can generally be influenced by crystallinity and particle size and shape, it is not surprising that some differences, such as shifts in the decomposition temperatures, are observed between mineral and synthetic samples. The rough agreement between experimental and calculated mass loss for all samples confirms the notional anionic composition. However, some features, such as the nature and varying fractions of high-temperature carbonate and the diversity of decomposition steps at low temperature, observed for the synthetic samples remain to be explained.

X-ray Diffraction

The experimental powder diffraction pattern of our malachite mineral sample is in excellent agreement with literature data based on the crystal structure described above (Figure 4, a). The XRD pattern of rosasite also agrees well with that calculated from the crystallographic data given by Perchiazzi[16] (Figure 4, b). In the case of mineral aurichalcite, the peak positions in the experimental powder XRD pattern are in good agreement with the literature pattern (Figure 4, c), although significant deviations are observed for the intensity ratios of some reflections, with a higher than expected intensity being observed, for example, for 020, $\bar{1}21$, $\bar{2}21$ and 040. [010] has been reported to be an axis of prominent crystal growth for aurichalcite.[27]

As expected, the precipitated samples are less crystalline, as indicated by the broad reflections and high background of the XRD patterns. However, a qualitative agreement between the XRD pattern of the minerals and the precipitated samples can be observed (Figure 4, a and c). Only one crystalline phase is present in each synthetic sample, namely aurichalcite for Cu/Zn = 1:2 and zincian malachite for Cu/Zn = 9:1. While the peak heights in the synthetic aurichalcite pattern are in agreement with those in the literature pattern, a pronounced anisotropic peak broadening is observed for the synthetic sample, with the reflections indexed at 020, 220 and 040, for example, appearing much sharper than the other peaks. To estimate the amount of amorphous material possibly present in the precipitated samples XRD patterns of an exact 50 wt.-% mixture of the samples and NaCl standard were recorded and subjected to two-phase Rietveld refinements (spiking method). Due to the much stronger peak intensities of the well crystallised NaCl standard, the sample peaks are not very well defined in the spiked mixture. Thus, the peak shape and lattice parameters of the sample compounds were first refined on the pattern of the pure sample (selected data are given in Table 1) and consecutively kept fixed to the obtained values during refinement of the data for the spiked samples. The amount of NaCl in the spiked samples was determined to be 55% and 50% of crystalline material, which corresponds to amorphous fractions of approximately 19% and 0% for the original samples of synthetic zincian malachite and aurichalcite, respectively. In the case of zincian malachite, the presence for amorphous phases may explain some of the deviations of the thermal properties between mineral reference and synthetic sample. However, the synthetic aurichalcite sample does not contain a significant amount of amorphous material.

The synthetic sample with a Cu/Zn ratio of 9:1 was identified as zincian malachite rather than rosasite as the composition is closer to malachite considering the minimal Zn content of 33% for natural rosasite, and the peak positions

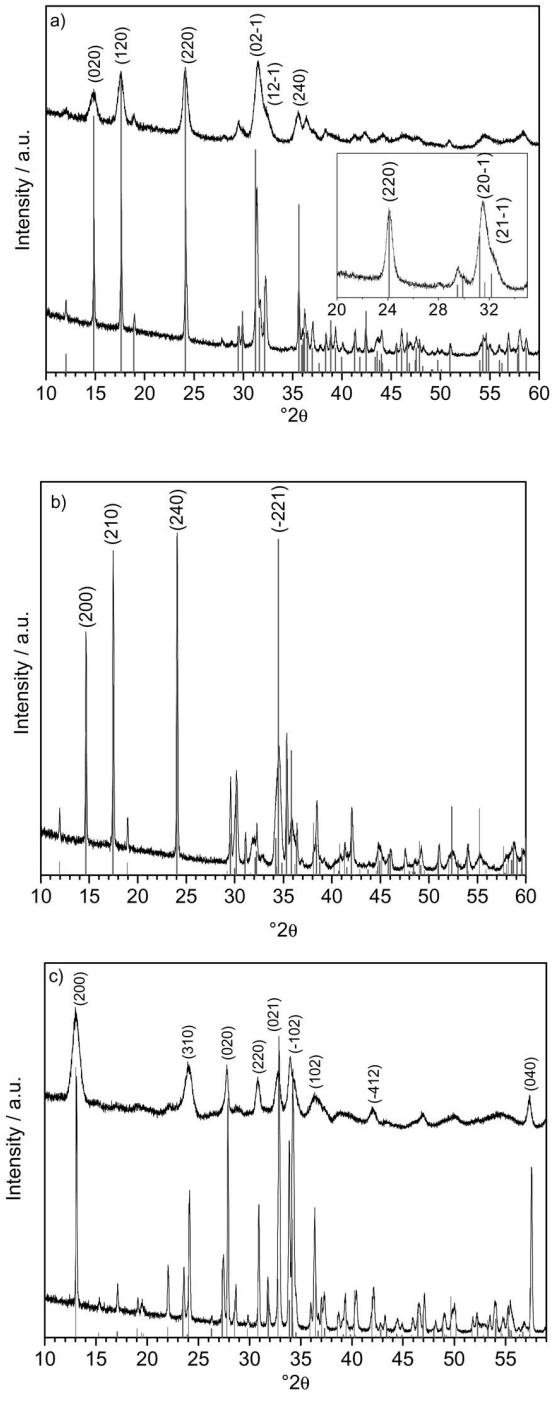

Figure 4. XRD patterns of: a) mineral malachite (bottom), synthetic zincian malachite (top) and calculated pattern (grey bar graph), b) mineral rosasite and calculated pattern (grey bar graph), c) mineral (bottom) and synthetic (top) aurichalcite and calculated pattern (grey bar graph).

of the precipitated zincian malachite sample are in significantly better agreement with the theoretical XRD pattern of malachite than with the pattern of rosasite, especially in the angular range 30–40° 2θ. Nevertheless, a considerable shift is observed for the 20$\bar{1}$ and the 21$\bar{1}$ peaks at 31.5° and 32.5° 2θ (the latter being present as a shoulder at the higher

Table 1. Selected results of the Rietveld fits of synthetic zincian malachite, aurichalcite and the catalyst precursor mixture. Structural models were taken from single-crystal data, and all atomic coordinates were refined.

	Zincian malachite Cu/Zn = 90:10	Aurichalcite[a] Cu/Zn = 33:67	Catalyst precursor Cu/Zn = 70:30
R_p/R_p'[b]	7.06/21.20	8.44/19.44	7.54/17.41
R_{wp}/R_{wp}'[b]	9.16/21.83	10.76/21.02	9.48/19.27
R_{exp}/R_{exp}'[a]	7.15/17.05	7.38/14.42	7.94/16.14
GOF/DW[c]	1.28/0.92	1.46/0.73	1.19/1.05
Aurichalcite			
R_{Bragg}		3.878	3.809
wt.-%[d]		100	14.5(3)
a [Å]		13.792(3)	13.751(5)
b [Å]		6.4238(7)	6.4309(19)
c [Å]		5.2851(10)	5.275(2)
β [°]		100.64(3)	99.56(3)
Malachite			
R_{Bragg}	3.537		2.967
wt.-%[d]	100		85.5(3)
a [Å]	9.5018(17)		9.3957(13)
b [Å]	11.999(2)		12.0622(18)
c [Å]	3.2291(5)		3.1877(4)
β [°]	98.548(10)		96.450(8)

[a] Fit accounting for anisotropic (i.e. *hkl*-dependent) peak broadening. [b] Primed R values are background-corrected; definition of the R values according to Young.[29] [c] DW = Durbin–Watson parameter.[30] [d] wt.-% from Rietveld fit. See text for estimation of amorphous fraction from spiked pattern.

angle side of the former) compared to the calculated malachite pattern, while all other peaks are in good agreement (Figure 4, see inset a). The shift of these two reflections towards higher angles is indicative of a decrease of the corresponding d-spacing and is correlated to Zn^{2+} incorporation into the malachite structure, as has been reported earlier for the 20$\bar{1}$ peak.[5,12]

Figure 5 shows that the Jahn–Teller-elongated axes of four out of the eight CuO_6 octahedra in the malachite unit cell are orientated nearly perpendicular to the (20$\bar{1}$) lattice planes (drawn in light grey in Figure 5), whereas the other four octahedra (two M1- and two M2-centered units each) are aligned with their elongated axis almost perpendicular to (21$\bar{1}$) (drawn in dark grey in Figure 5). This characteristic of the (20$\bar{1}$) planes lying nearly parallel to the equatorial Cu–O planes of the CuO_6 octahedral units in malachite has been reported previously and was related to crystal morphology and cleavage properties.[13,28] The orientation of the elongated axes (determined as straight lines between the axial O-atom positions) among the four octahedra within each of the groups differs only by 0° and 8.0° and the geometric deviations from the plane normals are 11.5° and 18.7° for (20$\bar{1}$) and 7.6° for (21$\bar{1}$). Thus, in a simplified picture, the d-spacing of (20$\bar{1}$) and (21$\bar{1}$) can be regarded as being correlated to the average Jahn–Teller-elongated Cu–O distances in the malachite structure. Zn^{2+}, which is a d^{10} ion, has different coordination requirements to Cu^{2+} (d^9) and is not a Jahn–Teller ion. Hence, the contraction of the lattice spacing in the directions perpendicular to (20$\bar{1}$) and (21$\bar{1}$) can be explained by an average contraction of the elongated axial M–O distances as a result of the net re-

duction of Jahn–Teller distortion of the metal oxygen octahedra as Cu^{2+} ions are substituted by Zn^{2+}. The shift of these two reflections is therefore a direct measure of the degree of incorporation of divalent non-Jahn–Teller ions – Zn^{2+} in our case – into the malachite structure. Due to the similar ionic radii of Cu^{2+} and Zn^{2+} and the limited flexibility of the crystal structure in the dense equatorial directions, the shift of all other reflections observed in the 2θ range 5–80° is much weaker. An overall shrinking of the unit cell volume with Zn^{2+} incorporation into the malachite lattice has been observed previously by Porta et al.[5] and the crystal field effect suggested here might serve as an explanation.

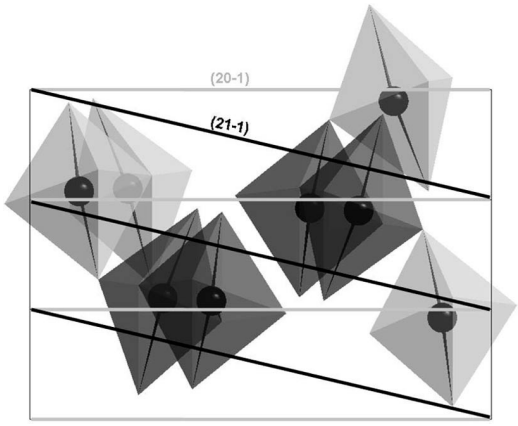

Figure 5. Unit cell of malachite with a set of $(20\bar{1})$ (grey) and $(21\bar{1})$ planes (black), viewed down $(50\bar{1})$, i.e. perpendicular to the plane normals. Only the axially elongated Cu–O bonds of the CuO_6 octahedra are drawn.

This simple correlation of Zn incorporation into malachite and the characteristic d-spacing of the $20\bar{1}$ peak has already been discussed previously,[12] but without structural interpretation. A plot of $d_{20\bar{1}}$ vs. nominal copper content (as [Cu]/[Cu+Zn] × 100%) for our samples is shown in Figure 6 together with some data taken from a paper by Bems et al.[12] for samples prepared by constant and decreasing pH co-precipitation. It can be seen that the range of existence of phase-pure zincian malachite ranges from 89% to 100% for samples prepared by deceasing pH precipitation, whereas for constant pH precipitation it ranges from 72% to 100%. This confirms that constant pH co-precipitation is the superior preparation method if a high degree of substitution is desired, for example for preparation of Cu/ZnO catalysts of high dispersion. For lower nominal Cu contents, $d_{20\bar{1}}$ is constant, thus indicating that no more Zn is incorporated into the malachite structure. At this point, aurichalcite starts to form as a Cu-poorer by-phase. It is interesting to note that the critical composition of 28 at.-% Zn falls below, but is still relatively close to, the lower compositional limit of natural rosasite of 33 at.-%, which cannot be reached by co-precipitation. The benefit of the technical catalyst composition of around 70:30 for Cu/Zn in combination with the constant pH technique is evident from Figure 6: maximal incorporation of Zn into the zincian malachite precursor phase is guaranteed by going below the critical composition near 72%, but large quantities of aurichalcite are avoided by closely approaching this composition. In this way, a high dispersion of copper in the final catalyst is achieved due to the uniform distribution of Cu and Zn in a Cu-rich precursor phase, while the contribution of Cu-poorer aurichalcite to the catalyst's weight is limited.

It can be seen from Figure 6 that at the same composition $d_{20\bar{1}}$ is generally larger for samples prepared at decreasing pH than for those prepared at constant pH, thereby indicating that the mode of preparation also affects the structure of the precipitate, for example due to formation of amorphous phases. Furthermore, it should also be noted

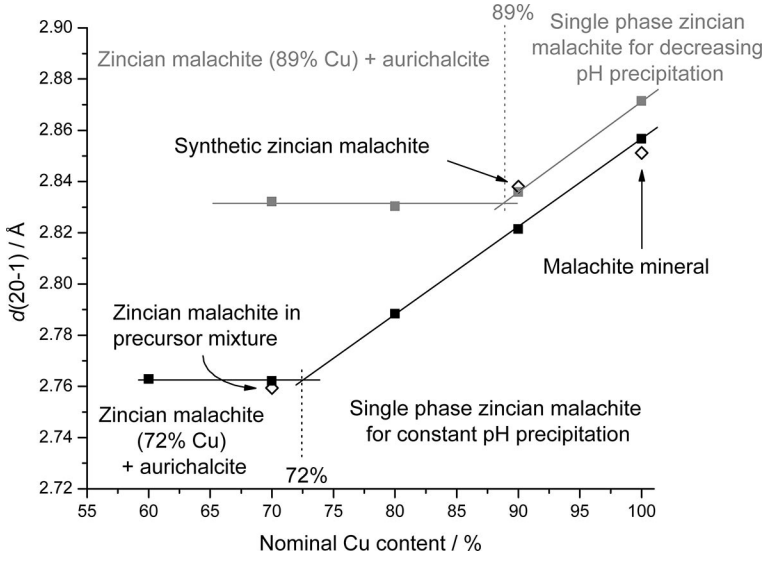

Figure 6. Plot of the d-spacing of the $(20\bar{1})$ planes vs. nominal Cu content {as [Cu]/([Cu]+[Zn])} for the samples in this study (open symbols) and data for samples prepared by constant (black) and decreasing pH (grey) precipitation taken from Bems et al.[12] (the data point at 90% Cu, decreasing pH, has been re-evaluated taking into account the neighbouring $21\bar{1}$ reflection).

that the pH[10,11] and the duration of the ageing period[2] have been shown to influence the phase composition and the Zn distribution in the precipitate.

The crystal structure of rosasite is different from the malachite structure. However, both phases are hard to discriminate by powder XRD, especially in the low-angle range which typically serves as a "fingerprint region" for phase identification in poorly crystalline catalyst precursor mixtures (Figure 7). Nevertheless, a reliable distinction is possible in the angular range 30–40° 2θ, where the rosasite structure exhibits unique reflections indexed as $\bar{2}21$ and 021. These reflections exhibit an extraordinary broadening and an intensity ratio and relative positions similar to the $20\bar{1}$ and $21\bar{1}$ peaks in malachite, although they are observed at much higher angles (34.5° and 35.9° 2θ, respectively). Hence, the position of these two characteristic reflections can serve as an indicator for the crystallographic phase (zincian malachite or rosasite)− for rosasite they are observed beyond 34° 2θ, whereas for (zincian) malachite both peaks can be found in the region below 34° 2θ. It is interesting to note that careful inspection of the XRD pattern of the rosasite mineral sample reveals the presence of two reflections at 31.9° and 32.8° 2θ (arrows in Figure 7), which cannot be explained by the rosasite crystal structure (see Figure 4, b). These reflections might rather be due to the $20\bar{1}$ and $21\bar{1}$ peaks of zincian malachite, thereby suggesting the presence of domains with the malachite structure in our rosasite sample. From their position, the Cu content of these domains can be estimated to be roughly 80% according to Figure 6, which clearly exceeds the average Cu content of this sample of 62%. It can be speculated that, similar to the precipitation system, a limiting Zn concentration for the malachite-like structure exists in the mineral, with the difference being that rosasite can be formed as a Cu-poorer by-phase, whereas upon precipitation it is aurichalcite.

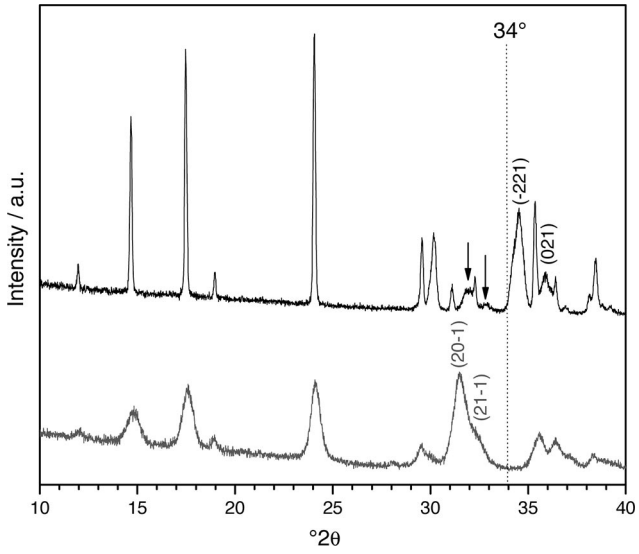

Figure 7. Comparison of the XRD patterns of mineral rosasite (black) and synthetic zinican malachite (grey), showing that the indexed reflections around 34° 2θ are useful for phase discrimination, while the peak positions match well at lower angles.

The Technical Precursor Mixture

The technical precursor mixture was prepared with a Cu/Zn ratio of 70:30 at a constant pH of 6.5. The XRD pattern is shown in Figure 8. A malachite-like and an aurichalcite-like phase can be identified. The single and quite sharp $20\bar{1}$ reflection observed at 32.4° 2θ indicates the presence of a single zincian malachite phase and a homogeneous Zn distribution in this phase and that pure malachite is absent. From its position well below 34° 2θ and the lack of any other unidentified peak near 34.5° 2θ, the presence of rosasite can be excluded. In addition, the broad IR band at 666 cm^{-1} indicative of rosasite is absent. A quantitative phase analysis by Rietveld refinement using 50 wt.-% NaCl as internal standard revealed a phase composition of 86 wt.-% zincian malachite, 14 wt.-% aurichalcite and 0 wt.-% X-ray amorphous material. Figure 8 shows the graphical results of the refinement for the unspiked pattern. Further data are given in Table 1. The IR spectroscopic results are in agreement with the phase composition determined by XRD. The IR spectrum of the precursor material is dominated by bands characteristic for the malachite-like structure and confirms the high content of this phase within the mixture (Figure 9). The fingerprint bands of aurichalcite are weak, but clearly present, at 1206 and 975 cm^{-1}. Additionally, two $\nu_2(CO_3^{2-})$ bands can be resolved: that at 832 cm^{-1} is assigned to aurichalcite and the stronger one at 820 cm^{-1} to zincian malachite.

The TG-MS curve of the precursor mixture is shown in Figure 10. The total mass loss is 27.9%, which is exactly the value expected for pure zincian malachite (assuming an average composition of Cu/Zn = 70:30, compared to 26.2% expected for pure aurichalcite). Again, the decomposition can be divided into two regions: after emission of physisorbed water around 100 °C, simultaneous emission of water and carbon dioxide is observed in the temperature range 150–400 °C and successive emission of high-temperature carbonate at 450–500 °C. The first region consists of at least four different poorly resolved decomposition steps, thereby reflecting the high chemical diversity of the precursor mixture compared to the minerals or physical mixtures thereof. The fraction of high-temperature carbonate is approximately 50% of the total carbonate content.

The Zn content of the zincian malachite phase can be estimated from the d-spacing of the $20\bar{1}$ reflection to have reached the maximum value of approximately 72 at.-% (Figure 6). Taking into account the relatively high Zn content of 28 at.-% of all metal species in the zincian malachite phase on the one hand, and the fraction of aurichalcite phase of 14 wt.-% determined by XRD on the other, a total metal composition of 70:30 is not even possible if the maximum Cu content of 40 at.-% for aurichalcite is assumed. For instance, a possible composition of the precursor mixture that satisfies the overall 70:30 ratio of Cu/Zn would be 95 wt.-%$[(Cu_{0.72}Zn_{0.28})_2(CO_3)(OH)_2]$ + 5 wt.-%$[(Cu_{0.4}Zn_{0.6})_5(OH)_6(CO_3)_2]$. The amount of aurichalcite present therefore appears to be overestimated by XRD. In addition to the general error that can be expected for the phase content of the minor phase in a poorly crystalline mixture, this overes-

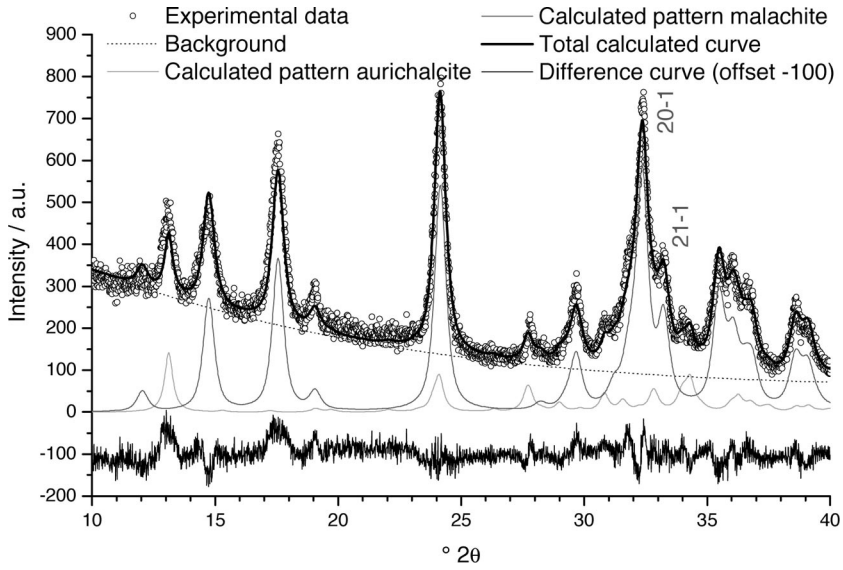

Figure 8. Phase refinement of the XRD pattern of the catalyst precursor mixture (section).

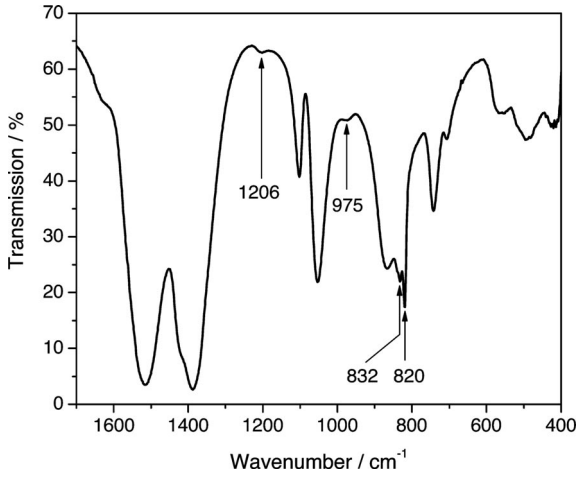

Figure 9. IR spectrum of the catalyst precursor mixture in the range 1700–400 cm^{-1}.

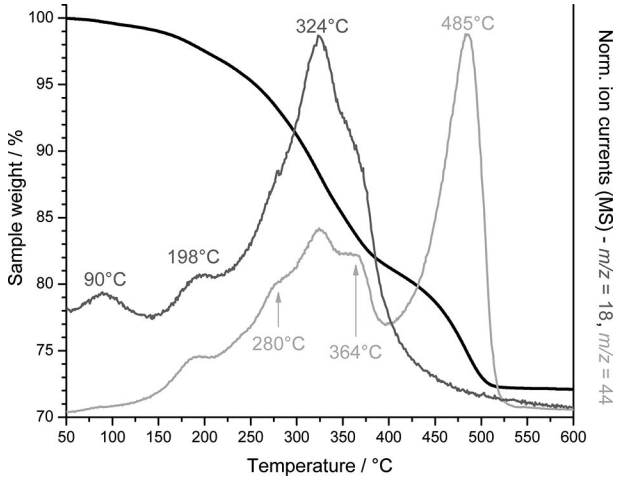

Figure 10. TG curve (black) and EGA traces for *m*/*z* 18 (dark grey) and *m*/*z* 44 (light grey) for the catalyst precursor mixture.

timation might be due the unusual intensity distribution observed for some reflections in the case of synthetic aurichalcite, which introduces further uncertainty in the quantitative XRD refinement. Moreover, in light of the limited number of reference samples and the fact that the presence of amorphous phases was neglected when plotting Figure 6, the error in the critical composition of the zincian malachite phase must be estimated to be at least ±5 at.-%. It should be kept in mind that these drawbacks may change the picture regarding the phase composition in the mixture as well as the metal composition of the single phases significantly.

Conclusions

The main conclusions of this study of mineral and synthetic mixed basic CuZn carbonates are as follows. The characteristic IR bands and XRD peaks render these methods suitable fingerprint methods for identification of (zincian) malachite, rosasite and aurichalcite. Furthermore, the shift of the $20\bar{1}$ and $21\bar{1}$ reflections of the malachite structure as a function of Zn incorporation can be understood on the basis of a simplified crystal field model involving a decrease of the average Jahn–Teller distortion of the MO_6 octahedra as Zn replaces Cu. The amorphous phases present in the synthetic zincian malachite sample introduce chemical diversity, which is reflected in the complex decomposition behaviour in the temperature range below 400 °C. The presence of so-called high-temperature carbonate (emitted at $T > 400$ °C) is not unique to precipitated samples and is also observed for minerals, which means that it cannot be related to amorphous by-phases. The malachite-like (Cu,Zn) phase in the catalyst precursor does not reach the substitution level of natural rosasite and should be termed zincian malachite rather than rosasite.

Using the mineral model strategy, in other words considering the complex technical catalyst precursor to be a physical mixture of mineral reference phases, successfully

simplifies the description of the catalyst precursor. However, in light of the complexity of the system, which also includes parameters not considered in this study, such as the pH of precipitation or duration of the ageing period, this provides only a very rough picture of the real situation. Complementary information on the metal composition of the single phases and on the chemical diversity introduced by the preparation process is therefore desirable for a comprehensive understanding.

The careful use of complementary analytical techniques such as IR spectroscopy, TGA and XRD provides valuable insights into the complex chemistry of the technical precursor mixture and means that an approximate estimation of the phase composition and the metal composition of the zincian malachite and aurichalcite phase is possible. It should be noted, however, that the accuracy of this estimation is governed by the limited number and general drawbacks of the analytical methods applied and the limited number of datasets for mineral and synthetic reference samples used in this study.

Experimental Section

General: Mineral samples were obtained from the mineral collection of the Technical University of Berlin. Synthetic zincian malachite was prepared by decreasing pH co-precipitation at 65 °C, as described previously,[12] from 1 M Cu,Zn nitrate solution and 1.2 M sodium carbonate solution. A high Cu/Zn ratio of 9:1 was chosen in order to avoid formation of aurichalcite as a by-phase. The precipitate was aged in the mother liquor for 3 h, washed thoroughly with bi-distilled water and dried at 60 °C overnight. Synthetic aurichalcite was prepared accordingly, but with a Cu/Zn ratio of 1:2. No indications of the presence of other phases were found for these samples. The technical precursor mixture was prepared according to an industrially applied procedure by a constant pH co-precipitation at pH 6.5 from a 1 M Cu/Zn nitrate solution with a ratio of 70:30 using 1.2 M sodium carbonate solution as precipitating agent. The precipitate was aged for 3 h in the mother liquor, washed and spray-dried.

The X-ray diffraction (XRD) measurements were performed with a STOE STADI P transmission diffractometer equipped with a primary focusing Ge monochromator (Cu-$K_{\alpha 1}$ radiation) and position-sensitive detector. The samples were mounted in the form of a clamped sandwich of small amounts of powder fixed with a small amount of grease between two layers of thin polyacetate film. Refinements were done in the 2θ range 5–90° using the software package TOPAS.[31] IR spectra were recorded with a FTIR Perkin–Elmer model 2000 using the KBr disc technique. Thermal analyses were performed with a NETZSCH STA449 thermobalance under a controlled flow of 20% O_2 in Ar with approximately 20 mg of sample at a heating rate of 2 °C min^{-1}. The gases evolved in the thermal analyses were monitored with a quadrupole mass spectrometer (QMS200 Omnistar, Balzers) coupled to the thermal balance via a quartz capillary.

Acknowledgments

The help of Dr. Andreas Furche, Edith Kitzelmann, Gisela Weinberg, Jutta Kröhnert, Nicole Hensel, and Dr. Rolf Jentoft with various characterisations is greatly acknowledged. We thank the Technical University Berlin for providing the mineral samples and the German Bundesministerium für Bildung und Forschung (BMBF) for financial support (BMBF project no. 01RI0529).

[1] P. B. Himmelfarb, G. W. Simmons, K. Klier, R. G. Herman, *J. Catal.* **1985**, *93*, 442.
[2] D. Waller, D. Stirling, F. S. Stone, M. S. Spencer, *Faraday Discuss. Chem. Soc.* **1989**, *87*, 107.
[3] G. C. Shen, S.-I. Fujita, N. Takezawa, *J. Catal.* **1992**, *138*, 754.
[4] F. S. Stone, D. Waller, *Top. Catal.* **2003**, *22*, 305.
[5] P. Porta, S. De Rossi, G. Ferraris, M. Lo Jacono, G. Minelli, G. Moretti, *J. Catal.* **1988**, *109*, 367.
[6] P. Porta, G. Fierro, M. Lo Jancono, G. Moretti, *Catal. Today* **1988**, *2*, 675.
[7] J.-L. Li, T. Inui, *Appl. Catal. A* **1996**, *137*, 105.
[8] G. J. Millar, I. H. Holm, P. J. R. Uwins, J. Drennan, *J. Chem. Soc. Faraday Trans.* **1998**, *94*, 593.
[9] D. M. Whittle, A. A. Mirzaei, J. S. J. Hargreaves, R. W. Joyner, C. J. Kiely, S. H. Taylor, G. J. Hutchings, *Phys. Chem. Chem. Phys.* **2002**, *4*, 5915.
[10] C. Kiener, M. Kurtz, H. Wilmer, C. Hoffmann, H.-W. Schmidt, J.-D. Grunwaldt, M. Muhler, F. Schüth, *J. Catal.* **2003**, *216*, 110.
[11] C. Baltes, S. Vukojevic, F. Schüth, *J. Catal.* **2008**, *258*, 334.
[12] B. Bems, M. Schur, A. Dassenoy, H. Junkes, D. Herein, R. Schlögl, *Chem. Eur. J.* **2003**, *9*, 2039.
[13] P. Süsse, *Acta Crystallogr.* **1967**, *22*, 146.
[14] F. Zigan, W. Josig, H. D. Schuster, *Z. Kristallogr.* **1977**, *145*, 412.
[15] A. C. Roberts, *Powder Diffraction* **1986**, *1*, 56.
[16] N. Perchiazzi, *Z. Kristallogr. Suppl.* **2006**, *23*, 505.
[17] M. M. Harding, B. M. Kaiuki, R. Cernik, G. Cressey, *Acta Crystallogr., Sect. B* **1994**, *50*, 673.
[18] C. Palache, H. Berman, C. Frondel, in *Dana's System of Mineralogy*, J. Wiley & Sons, New York, **1951**.
[19] *Carbonates* (Eds.: R. J. Meyer, E. H. E. Pietsch, A. Kotowski), Gmelin Institut für Anorganische Chemie, Verlag Chemie, Weinheim, **1955**, p. 173.
[20] M. Schmidt, H. D. Lutz, *Phys. Chem. Minerals* **1993**, *20*, 27.
[21] R. S. W. Braithwaite, G. R. Ryback, *J. Mineral. Soc.* **1963**, *261*, 441.
[22] D. Stoilova, V. Koleva, V. Vassileva, *Spectochim. Acta A* **2002**, *58*, 2051.
[23] R. S. W. Braithwaite, *Mineral. Magn.* **1963**, *33*, 441.
[24] K. Nakamoto, in *Infrared Spectra of Inorganic and Coordination Compounds*, J. Wiley & Sons, New York, **1963**.
[25] J. A. Goldsmith, S. D. Ross, *Spectrochim. Acta A* **1968**, *24*, 2131.
[26] M. Schur, B. Bems, A. Dassenoy, I. Kassatkine, J. Urban, H. Wilmes, O. Hinrichsen, M. Muhler, R. Schlögl, *Angew. Chem. Int. Ed.* **2003**, *42*, 3815.
[27] J. W. Anthony, R. A. Bideaux, K. W. Bladh, M. C. Nichols, in *Handbook of Mineralogy*, Mineral Data Publishing, Tiscon, **2003**.
[28] A. F. Wells, *Acta Crystallogr.* **1951**, *4*, 200.
[29] *The Rietveld Method* (Ed.: R. A. Young), Oxford University Press, Oxford, **1993**, p. 1.
[30] R. J. Hill, H. D. Flack, *J. Appl. Crystallogr.* **1987**, *20*, 356.
[31] A. A. Coelho, *Topas, General Profile and Structure Analysis Software for Powder Diffraction Data*, Version 3.0, Bruker AXS GmbH, Karlsruhe, Germany, **2006**.

Received: December 17, 2008
Published Online: February 26, 2009

